

# Visualization Method to Predict the Nucleophilic Asymmetric Induction of Prochiral Electrophiles

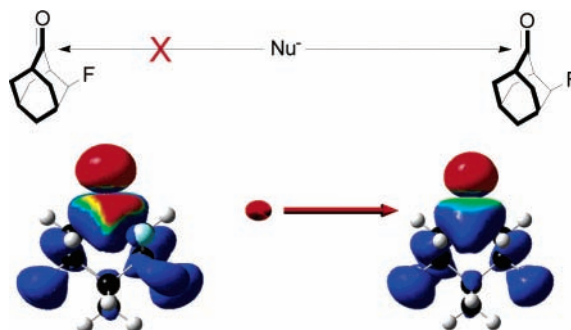
Nathan Wilmot and Michael J. Marsella\*

Department of Chemistry, University of California at Riverside,  
Riverside, California 92521

michael.marsella@ucr.edu

Received May 18, 2006

## ABSTRACT



This work focuses on the development of a simple technique to accurately predict and visualize the diastereoselectivity of ketone, aldehyde, and allyl chloride reductions by mapping electrostatic potential onto the frontier molecular orbital involved in the reduction. A distinct difference of electrostatic potential on the faces of the carbonyl can be used to predict the face of nucleophilic attack with a high level of accuracy.

Predicting the outcome of asymmetric induction during the reduction of aldehydes and ketones has been the subject of intense investigation since the pioneering work by Cram in 1952.<sup>1</sup> For prochiral carbonyls (and  $\alpha$ -chiral allyl chlorides) that are proximal to an asymmetric element, the Cram, Felkin–Anh, and related noncomputational models work with remarkable success.<sup>2–9</sup> This is a particularly interesting fact given that biased conformations (as opposed to true

global conformational minima) are often required by rule. More precise analysis can be ascertained using computational chemistry, albeit with greater effort, as transition states can be located and relative energies can be compared.<sup>10–15</sup>

Herein, we report a simple computational method to predict asymmetric induction via visual inspection of a single, mapped isosurface. This method is not intended to be a quantitative and rigorous theoretical treatment of asymmetric induction, but rather a broadly applicable, qualitative method that requires minimal computational time (minutes) to project

(1) Cram, D. J.; Elhafez, F. A. A. *J. Am. Chem. Soc.* **1952**, *74*, 5828–5835.

(2) Eisenstein, O.; Hoffmann, R. *J. Am. Chem. Soc.* **1980**, *102*, 6148–6149.

(3) Eisenstein, O.; Lefour, J. M.; Anh, N. T.; Hudson, R. F. *Tetrahedron* **1977**, *33*, 523–531.

(4) Anh, N. T.; Eisenstein, O. *Tetrahedron Lett.* **1976**, 155–158.

(5) Cherst, M.; Felkin, H.; Prudent, N. *Tetrahedron Lett.* **1968**, *18*, 2199–2204.

(6) Cornforth, J. W.; Cornforth, M. R. H.; Methew, K. K. *J. Chem. Soc.* **1959**, 1959, 112–127.

(7) Karabotsos, G. J. *Tetrahedron Lett.* **1972**, *52*, 5289–5292.

(8) Karabotsos, G. J.; T. H. *Tetrahedron Lett.* **1967**, *49*, 4911–4914.

(9) Karabotsos, G. J. *J. Am. Chem. Soc.* **1967**, *89*, 1367–1371.

(10) Anh, N. T.; Eisenstein, O.; Lefour, J.-M.; Dau, M.-E. T. H. *J. Am. Chem. Soc.* **1973**, *95*, 6146–6147.

(11) Wu, Y. D.; Houk, K. N. *J. Am. Chem. Soc.* **1987**, *109*, 908–910.

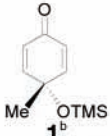


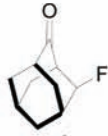


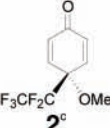


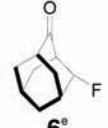


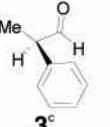


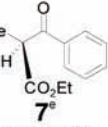
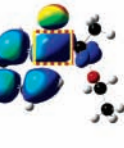
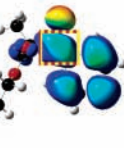
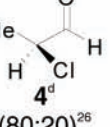


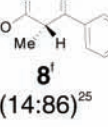


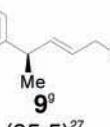


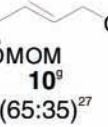


(12) Cee, V. J.; Cramer, C. J.; Evans, D. A. *J. Am. Chem. Soc.* **2006**, *128*, 2920–2930.

(13) Chao, I.; Shih, J. H.; Wu, H. J. *J. Org. Chem.* **2000**, *65*, 7523–7533.

(14) Paddon-Row, M. N.; Wu, Y.-D.; Houk, K. N. *J. Am. Chem. Soc.* **1992**, *114*, 10638–10639.

(15) Wu, Y. D.; Li, Y.; Na, J.; Houk, K. N. *J. Org. Chem.* **1993**, *58*, 4625–4628.

**Table 1.** Test Compound Electrostatic Potential Maps on LUMO<sub>E</sub> Surfaces<sup>a</sup>

2D-structure (exp. A:B ratio)	A-attack face	B-attack face	2D-structure (exp. A:B ratio)	A-attack face	B-attack face
 <b>1<sup>b</sup></b> (17.7:1) <sup>21</sup>			 <b>5<sup>°</sup></b> (100:0) <sup>22</sup>		
 <b>2<sup>c</sup></b> (1:5) <sup>21</sup>			 <b>6<sup>°</sup></b> (33:67) <sup>22</sup>		
 <b>3<sup>c</sup></b> (80:20) <sup>23,24</sup>			 <b>7<sup>e</sup></b> (75:25) <sup>25</sup>		
 <b>4<sup>d</sup></b> (80:20) <sup>26</sup>			 <b>8<sup>f</sup></b> (14:86) <sup>25</sup>		
 <b>9<sup>g</sup></b> (95:5) <sup>27</sup>			 <b>10<sup>h</sup></b> (65:35) <sup>27</sup>		

<sup>a</sup> Isosurface values = 0.02. Nucleophiles used in cited product ratios: <sup>b</sup> CH<sub>3</sub>MgBr. <sup>c</sup> CH<sub>3</sub>Li. <sup>d</sup> CH<sub>3</sub>MgCl. <sup>e</sup> NaBH<sub>4</sub>. <sup>f</sup> NaBH<sub>4</sub> + ZnCl<sub>2</sub>. <sup>g</sup> Bu<sub>2</sub>CuLi·ZnCl<sub>2</sub>.

a visual interpretation of the frontier molecular orbital (FMO) theory<sup>16</sup> onto a prochiral electrophile. In addition, this method does not require the user to infer steric arguments or calculate transition states, nor does it require biased conformations (only the geometry optimized, global minimum geometry is necessary). Despite a simplistic approach, it will be shown that the accuracy for predicting stereochemical outcome is excellent across a diverse group of molecules, including those with proximal and distant elements of chirality, as well as metal chelates.

Our strategy integrates the following concepts: (1) For any carbonyl functional group situated asymmetrically within a molecule, the asymmetry of its environment will be translated to associated molecular orbital topology, electron density, and electrostatic potential. This translation of asymmetry to electronic properties establishes, in part, the basis for prochiral facial selectivity by an attacking nucleophile.

(2) FMO theory teaches that the most significant interaction between a nucleophile and an electrophile is that of the HOMO and LUMO, respectively. Thus, our primary interest is the asymmetric topology of the lowest-unoccupied molecular orbital that exhibits an isosurface proximal to the reactive electrophilic site. Although this is typically the LUMO, there are some exceptions (noted below), thus we will refer to the orbital of interest as the LUMO<sub>E</sub>.

The three-dimensional LUMO<sub>E</sub> defines a “target” for nucleophilic attack but lacks a visually evident “bullseye” to be used as a predictor of facial selectivity. This issue can be satisfied by mapping onto the LUMO<sub>E</sub> the corresponding electrostatic potential (ESP). The concept of predicting nucleophilic attack using a map of ESP onto total molecular electron density is established.<sup>13,15</sup> However, we opt to focus specifically on the LUMO<sub>E</sub> isosurface, with the following rationale: (1) it conceptually parallels FMO theory; (2) it provides enhanced resolution of the reactive electrophile’s electrostatic environment (i.e., a more well-defined “bulls-

(16) Fukui, K. *Acc. Chem. Res.* **1971**, *4*, 57–64.

eye" for visual inspection); and (3) it avoids a formal consideration of the Bergi–Dunitz angle<sup>17–19</sup> of nucleophilic attack. The latter is rendered unnecessary as the angle of nucleophile approach should map onto that region of the LUMO<sub>E</sub> corresponding with the electrophilic center.

The Gaussian 03 suite of software<sup>20</sup> (G03W for calculations and GaussView for visualization) was employed as follows. First, a PM3 geometry optimization was performed on the conformation corresponding to the global minimum of the molecule of interest. Next, a HF/6-31G(d) single-point energy calculation was done using the structure determined from step 1. Last, the HF calculation allows one to generate an isosurface portraying the ESP mapped onto the LUMO<sub>E</sub>. Final analysis requires a visual inspection of the mapped isosurface, to determine the more electropositive face of the LUMO<sub>E</sub> (i.e., the darker blue isosurface). Note that the range of colors used to map ESP can be attenuated as needed to accentuate differences in color mapping.

Table 1 lists 10 compounds that were analyzed as described above (additional examples can be found in the Supporting Information). Each entry reports the two-dimensional structure, the experimentally reported diastereoselectivity, and the corresponding map of LUMO<sub>E</sub>–ESP for each of the two prochiral faces. For convenience, the area of the LUMO<sub>E</sub> proximal to the site of the electrophilic functional group (typically a carbonyl group) is highlighted with a box. The prochiral face showing the darkest blue color within the highlighted area is predicted to be the favored face for nucleophilic attack. As can be seen, experimental results validate the prediction in every case.

The classes of molecules studied are as follows:<sup>21–27</sup> (i) entries **1** and **2** have  $\gamma$ -chiral centers; (ii) entries **3** and **4** have  $\alpha$ -chiral centers; (iii) entries **5** and **6** are diastereomeric fluoroadamantanones ( $\beta$ -chiral center); (iv) entries **7** and **8** are  $\alpha$ -chiral, nonchelate, and chelate substrates (in this latter case, the LUMO<sub>E</sub> corresponds to the LUMO + 1, as the LUMO is centered on the zinc ion); and (v) entries **9** and **10** illustrate successful predictions with allyl chlorides as substrates. In each case, the color coding within the highlighted box (that area associated with the electrophilic carbon) shows a clear distinction between facial selectivity:

(17) Burgi, H. B.; Dunitz, J. D. *Acc. Chem. Res.* **1983**, *16*, 153–161.

(18) Burgi, H. B.; Dunitz, J. D.; Lehn, J. M.; Wipff, G. *Tetrahedron* **1974**, *30*, 1561–1572.

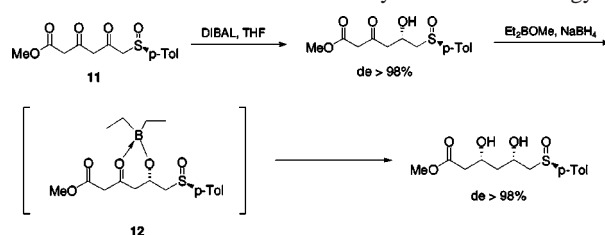
(19) Burgi, H. B.; Dunitz, J. D.; Shefter, E. *J. Am. Chem. Soc.* **1973**, *95*, 5065–5067.

(20) Frisch, M. J.; Trucks, G. W.; Schlegel, H. B.; Scuseria, G. E.; Robb, M. A.; Cheeseman, J. R.; Montgomery, J. A., Jr.; Vreven, T.; Kudin, K. N.; Burant, J. C.; Millam, J. M.; Iyengar, S. S.; Tomasi, J.; Barone, V.; Mennucci, B.; Cossi, M.; Scalmani, G.; Rega, N.; Petersson, G. A.; Nakatsuji, H.; Hada, M.; Ehara, M.; Toyota, K.; Fukuda, R.; Hasegawa, J.; Ishida, M.; Nakajima, T.; Honda, Y.; Kitao, O.; Nakai, H.; Klene, M.; Li, X.; Knox, J. E.; Hratchian, H. P.; Cross, J. B.; Bakken, V.; Adamo, C.; Jaramillo, J.; Gomperts, R.; Stratmann, R. E.; Yazyev, O.; Austin, A. J.; Cammi, R.; Pomelli, C.; Ochterski, J. W.; Ayala, P. Y.; Morokuma, K.; Voth, G. A.; Salvador, P.; Dannenberg, J. J.; Zakrzewski, V. G.; Dapprich, S.; Daniels, A. D.; Strain, M. C.; Farkas, O.; Malick, D. K.; Rabuck, A. D.; Raghavachari, K.; Foresman, J. B.; Ortiz, J. V.; Cui, Q.; Baboul, A. G.; Clifford, S.; Cioslowski, J.; Stefanov, B. B.; Liu, G.; Liashenko, A.; Piskorz, P.; Komaromi, I.; Martin, R. L.; Fox, D. J.; Keith, T.; Al-Laham, M. A.; Peng, C. Y.; Nanayakkara, A.; Challacombe, M.; Gill, P. M. W.; Johnson, B.; Chen, W.; Wong, M. W.; Gonzalez, C.; Pople, J. A. *Gaussian 03*, revision B.3; Gaussian, Inc.: Pittsburgh, PA, 2003.

a generic nucleophile will attack the more electron-deficient target (denoted as dark blue).

This method was extended to more complex compounds, with multiple ketones and more diverse substitutions, to further explore the method. The first example is a diketoester utilized by the Solladie group in the synthesis of a precursor of compactin and mevinolin.<sup>28,29</sup> The experimental result is shown in Scheme 1, and Table 2 shows the corresponding

**Scheme 1.** Solladie Diketoester Synthetic Methodology



LUMO<sub>E</sub>–ESP map. In agreement with experiment, the most reactive site is the *si*-face of the ketone situated  $\beta$  to the sulfoxide. The subsequent synthetic step uses Et<sub>2</sub>BOME as a chelating moiety, and this complex was modeled in our analysis. Visual inspection reveals a very distinct, preferred face of attack, again in full agreement with experiment.

**Table 2.** Solladie Diketoester LUMO<sub>E</sub>–ESP Maps<sup>a</sup>

compound	favored product face	disfavored product face
<b>11</b>		
<b>12</b>		

<sup>a</sup> Isosurface values = 0.02.

The final example analyzes the diastereoselective reduction of compound **13** (Scheme 2), as reported by Danishefsky<sup>30</sup> (Table 3). Compound **13** is subject to nucleophilic attack at the aldehyde carbon, and experimental results yield a diastereoselectivity of 67:33.

(21) Wipff, P.; Kim, Y. T. *J. Am. Chem. Soc.* **1994**, *116*, 11678–11688.

(22) Kaselj, M.; leNoble, W. J. *J. Org. Chem.* **1996**, *61*, 4157–4160.

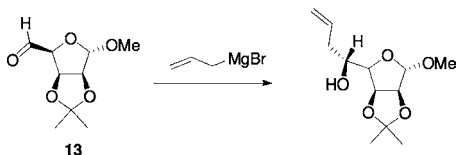
(23) Nakada, M.; Urano, Y.; Kobayashi, S.; Ohno, M. *J. Am. Chem. Soc.* **1988**, *110*, 4826–4827.

(24) Yamamoto, Y.; Maruyama, K. *J. Am. Chem. Soc.* **1985**, *107*, 6411–6413.

(25) Taniguchi, M.; Fujii, H.; Oshima, K.; Utimoto, K. *Tetrahedron* **1993**, *49*, 11169–11182.

(26) Frenking, G.; Kohler, K. F.; Reetz, M. T. *Tetrahedron* **1991**, *47*, 9005–9018.

(27) Arai, M.; Kawasuji, T.; Nakamura, E. *J. Org. Chem.* **1993**, *58*, 5121–5129.

**Scheme 2.** Danishefsky Aldehyde Synthetic Method

Once again, visual inspection of the LUMO<sub>E</sub>–ESP predicts the experimentally observed face of nucleophilic attack.

In summary, we have integrated readily available computations with visualization techniques to yield a simple and effective method to predict the preferred face of attack onto an asymmetric electrophilic carbon by a nucleophile. This method parallels concepts from FMO theory and should be applicable to visualizing asymmetric induction both in the laboratory and in the classroom.

(28) Solladie, G.; Bauder, C.; Rossi, L. *J. Org. Chem.* **1995**, *60*, 7774–7777.

(29) Chen, K. M.; Hardtmann, G. E.; Prasad, K.; Repic, O.; Shapiro, M. *J. Tetrahedron Lett.* **1987**, *28*, 155–158.

(30) Danishefsky, S. J.; Deninno, M. P.; Phillips, G. B.; Zelle, R. E.; Lartey, P. A. *Tetrahedron* **1986**, *42*, 2809–2819.

**Table 3.** Danishefsky Aldehyde LUMO<sub>E</sub>–ESP Maps<sup>a</sup>

compound	favored product face	disfavored product face
 13		

<sup>a</sup> Isosurface values = 0.02.

**Acknowledgment.** The authors acknowledge the University of California at Riverside for financial support.

**Supporting Information Available:** Further examples of the visualization method as well as Gaussian output files. This material is available free of charge via the Internet at <http://pubs.acs.org>.

OL061224A